Experimental Mechanics (2006) 46: 355–366
DOI 10.1007/s11340-006-6414-8

A Numerical Study of the Applicability of the Shear Compression Specimen to Parabolic Hardening Materials

A. Dorogoy · D. Rittel

Received: 6 July 2005 / Accepted: 14 November 2005 / Published online: 7 March 2006

Abstract This paper addresses *quasi-static* loading of the shear compression specimen (SCS), that has been especially developed to investigate the shear response of materials at various strain rates. Previous work [4, 5] addressed bi-linear hardening materials, whereas the present work concerns parabolic hardening materials. The investigation is done numerically using three-dimensional elastoplastic finite element simulations. The analyses show that the averaged von Mises stress ($\hat{\sigma}_{eq}$) and strain ($\hat{\varepsilon}_{eq}$) on a mid-section of the gauge reflect accurately the prescribed parabolic hardening model. A method for finding the parabolic hardening coefficients and reducing the measured load, P, and displacement, d, into equivalent stress $\hat{\sigma}_{eq}$ and strain $\hat{\varepsilon}_{eq}$ is introduced and tested. A very good agreement is observed, thus confirming the potential of the technique for large strain testing of parabolic hardening materials.

Keywords Large strain · Shear compression specimen · Parabolic hardening material · Finite elements · Constitutive · Quasi-static loading

Introduction

The shear compression specimen (SCS) developed by Rittel et al. [1, 2], was specially designed to investigate the mechanical behavior of materials at large strains, over a wide range of strain-rates. The main idea is that a single specimen geometry can be used to investigate both the quasi-static and the dynamic behavior of a material in a seamless fashion. The specimen, of a very simple geometric shape, consists basically of a cylinder or a parallelepiped with a couple of opposite slots machined at 45° on its faces. As the specimen is axially loaded (either dynamically or statically), the gauge (slot) experiences a dominant state of shear. However, as repeatedly emphasized, one should not assume a state of pure shear, as preliminary numerical calculations [1] clearly showed that the state of stress is three-dimensional. Consequently, the authors proposed to base the analysis on the Von Mises equivalent stress and strain definitions. The validity of the specimen was further established by comparing stress-strain data obtained with the SCS to those obtained from uniaxial (tension/compression) tests. While the first reports [1, 2] suggested simple "universal" approximations for the effective stress and strain, as a function of the load and displacement, respectively, further work suggested that these approximations must be fine-tuned to the material itself and to the gage geometry [3]. Quite recently, a thorough numerical investigation of the SCS for both quasi-static and dynamic loading conditions, was presented [4, 5]. Several issues such as homogeneity of the stresses and strains, stress-concentration and friction with the end-pieces, were addressed. In addition, the technique used to reduce the measured load and displacement data into equivalent stress-strain curves, was refined.

However, all the above-mentioned investigations rely on the basic assumption that the elastic-plastic

A. Dorogoy · D. Rittel (✉, SEM member)
Mechanical Engineering Department,
Technion–Israel Institute of Technology, 32000 Haifa, Israel
e-mail: merittel@technion.ac.il

flow behavior of the material can be adequately described by a *bi-linear* law. While this approximation is satisfactory as a first step, one important question remains unanswered as to the applicability of the SCS to *parabolic hardening* materials, which are quite common among metallic materials. The purpose of the present paper is to report new results about quasi-static loading of parabolic hardening materials, and the main outcome is that the SCS is suitable for the characterization of such materials.

The paper is organized as follows: first, the specimen geometry, material model and numerical details are introduced. Next, numerical results are presented. These results include P-d curves, $\hat{\sigma}_{eq} - \hat{\varepsilon}_{eq}$ curves and $\hat{\sigma}_{eqv} - P$ and $\hat{\varepsilon}_{eqv} - d$ curves. A hybrid numerical-experimental method for extracting the non linear material characteristics is then introduced. The following section describes numerical verification problems which demonstrate the applicability of the method. The results of this study are discussed, followed by concluding remarks.

Specimen Geometry and Material Data

The shear compression specimen (SCS) is shown in Fig. 1. The specimen promotes dominant shear deformation in an inclined gauge-section, and it is aimed at large-strain constitutive testing of materials, under both quasi-static and dynamic loading conditions [1–5]. For all the presently investigated cases, the length, diameter, gauge thickness, gauge height and root corner radius were chosen to be: L = 20 mm, D = 10 mm, t = 2.5 mm, w = 1.0 mm and r_1 = 0.25 mm respectively. This set of geometrical parameters is commonly used in experiments.

The specimen material is assumed to be elastic-plastic with a parabolic hardening behavior. The elastic

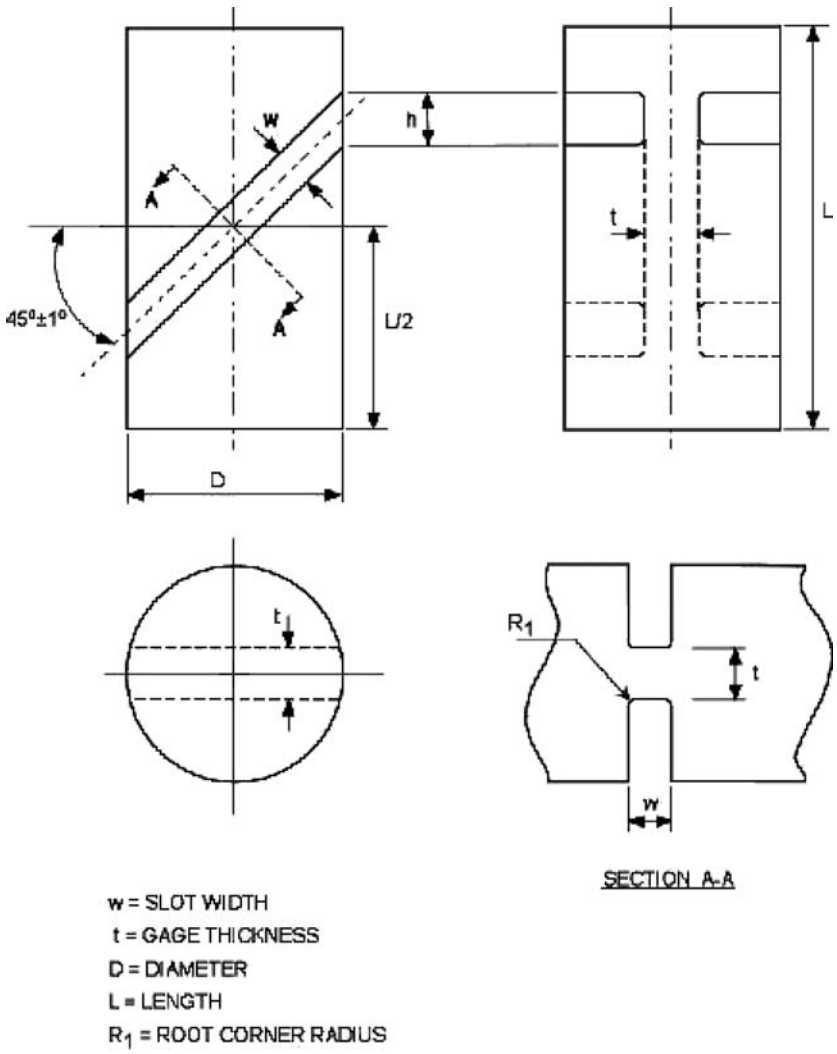

Fig. 1. The shear compression specimen

Table 1 Hardening parameters

Set	B [MPa]	*n*
#1	400	0.35
#2	600	0.35
#3	600	0.15

properties of the material were chosen to be: Young's modulus E = 210 GPa, Poisson's ratio $\nu = 0.3$ and yield stress $\sigma_Y = 0.91$ GPa. Isotropic hardening is assumed in which the yield stress σ^0 is described by

$$\sigma^0 = A + B(\bar{\varepsilon}^p)^n \tag{1}$$

where $\bar{\varepsilon}^p$ is the equivalent plastic strain while A, B and n are material parameters. A is the yield stress σ_Y. Three different sets of hardening parameters were examined, as detailed in Table 1.

Numerical Model

The numerical analysis was carried out using the commercial finite element code ANSYS [6]. A total of 15119 elements of type SOLID187 (3-D 10-node tetrahedral structural solid) were used to mesh the half specimen with 3803 elements in the gauge specifically. The meshed half specimen is seen in Fig. 2(a) and the half gauge mesh is detailed in Fig. 2(b). The boundary conditions, applied forces and numerical procedure are identical to those reported in previous work [4].

The parabolic hardening material model was approximated in ANSYS with the option MISO: multilinear isotropic hardening using von Mises plasticity. For practical implementation, the stress-strain curves were approximated by 16 linear segments. The pairs $(\sigma_i, \varepsilon_i)$ of the material model were calculated by

$$\sigma_i = \sigma_Y + B\left(\bar{\varepsilon}_i^p\right)^n \tag{2}$$

$$\varepsilon_i = \frac{\sigma_i}{E} + \bar{\varepsilon}_i^p \tag{3}$$

as shown in Fig. (3) for the models of Table 1. Each point in Fig. (3) represents an input data pair $(\sigma_i, \varepsilon_i)$. The first pair is of course $(\sigma_Y, \sigma_Y/E)$. It can be noticed in Fig. (3) that the linear segmentation yields a satisfactory representation of the parabolic curvature.

Results

First, we examine the equivalent von Mises stress (σ_{eqv}) and the equivalent total strain (ε_{eqv}) on the

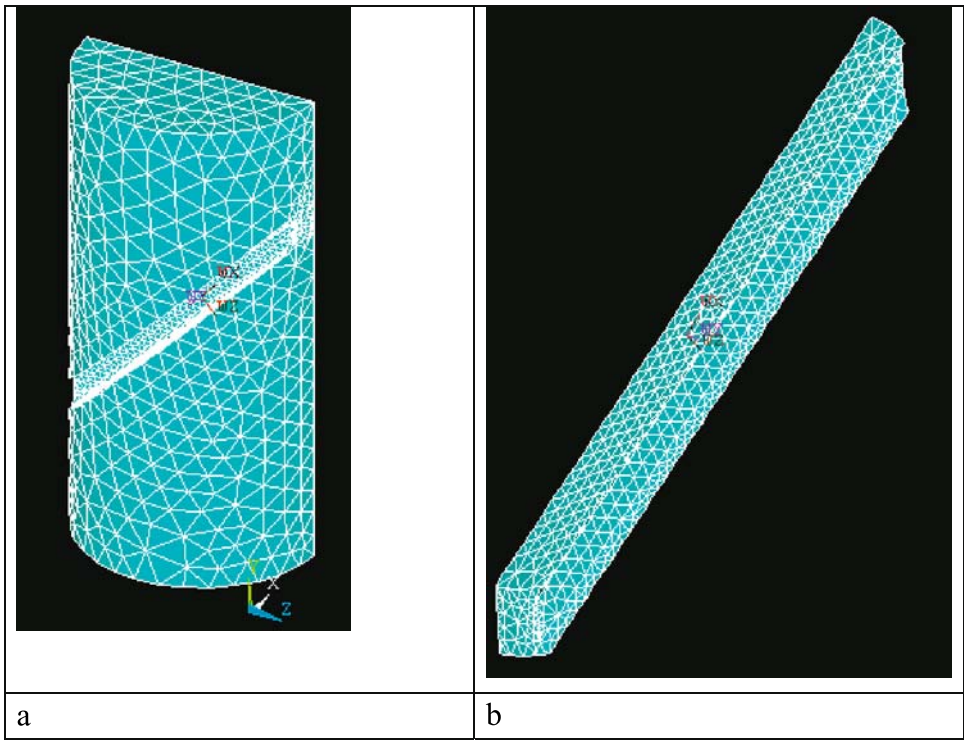

a b

Fig. 2. (**a**) The meshed half specimen. (**b**) The meshed half gage

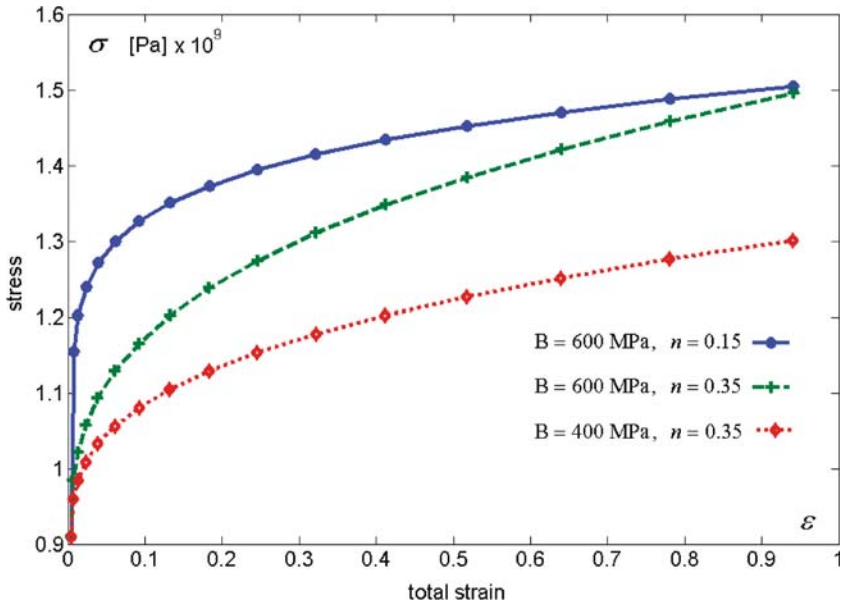

Fig. 3. (a) The parabolic hardening material models represented by ANSYS option MISO

inclined mid-section. Averaged values of $\hat{\sigma}_{eqv}$ and $\hat{\varepsilon}_{eqv}$ are calculated at each load step. The inclined mid-section of the gauge is shown in Fig. (4), where the upper half of the specimen has been removed. As in previous work [4, 5], the averaged values are calculated by integrating the stresses on the mid-section and dividing them by the area of the plane, according to:

$$\hat{\sigma}_{eqv} = \frac{1}{A}\int_A \sigma_{eqv}\, dA \tag{4}$$

$$\hat{\varepsilon}_{eqv} = \frac{1}{A}\int_A \varepsilon_{eqv}\, dA \tag{5}$$

The resulting $\hat{\sigma}_{eqv} - \hat{\varepsilon}_{eqv}$ for each load step are plotted in Fig. 5 and compared to the prescribed material models (Table 1) and equations (2)–(3). A very good agreement is observed. The values of $\hat{\sigma}_{eqv}$ are only 2% smaller than the prescribed σ^0 for the three investigated cases, and they all exhibit the prescribed curvature. This fact indicates that the prescribed constitutive relations are recovered by the average values of $\hat{\sigma}_{eqv}$ and $\hat{\varepsilon}_{eqv}$ for the three models. A similar conclusion was reached previously for the bi-linear material model [4].

The effect of parabolic hardening on the load-displacement curves, which are measured during an experiment, is considered next. The displacement d is the applied displacement of the upper face of the SCS, and the load P is the resultant applied force which is calculated by integrating the normal stresses over the upper face.

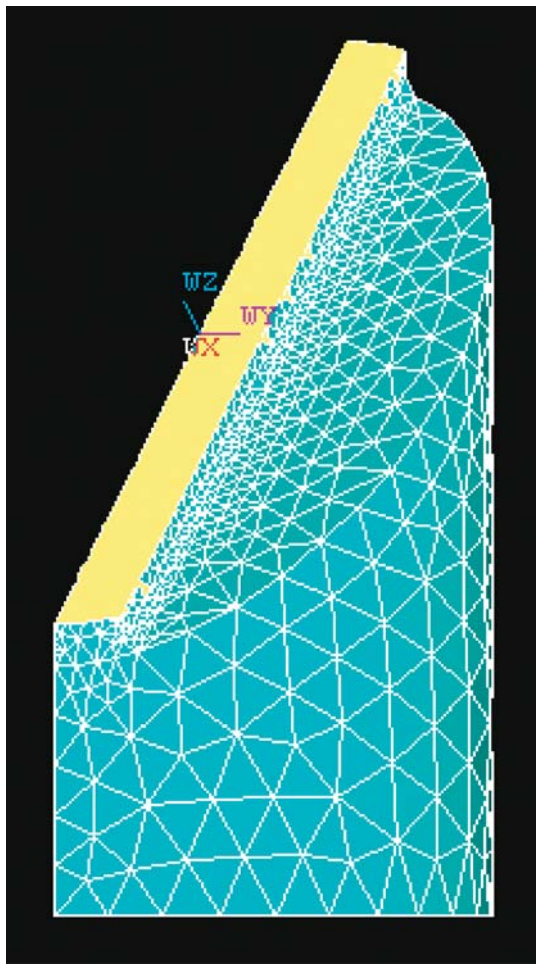

Fig. 4. The inclined mid-section of the gauge where the averaged $\hat{\sigma}_{eqv}$ and $\hat{\varepsilon}_{eqv}$ are calculated

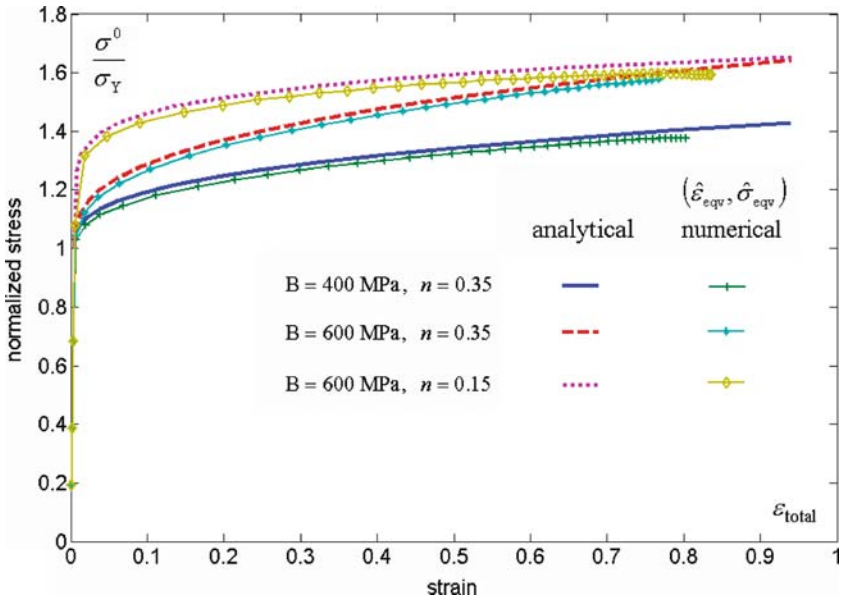

Fig. 5. A comparison between $\hat{\sigma}_{eqv}$ and $\hat{\varepsilon}_{eqv}$ to the prescribed models

Figure 6 shows a high level of similarity between the constitutive relation and the P-d curve. This similarity can be used to approximate the load displacement curve, for $P > P_Y$, as follows:

$$P = P_Y + C(d - d_Y)^k \tag{6}$$

Where (d_Y, P_Y) is the point on the load displacement curve at yield as indicated in Fig. 6. The coefficients C and k depend on the material hardening coefficients B and n.

Equation (6) can be re-written in the form

$$\log_{10}(P - P_Y) = \log_{10} C + k \log_{10}(d - d_Y) \tag{7}$$

Similarly, equation (1) can be re-written in the form

$$\log_{10}(\sigma^0 - \sigma_Y) = \log_{10} B + n \log_{10} \varepsilon^p \tag{8}$$

Figure 7 is a re-plot of the load-displacement curves of Fig. 6 according to equation (7). The resultant three straight lines indicate that the assumption of equation (6) is correct. Table 2 summarizes the input values of Table 1, in relation with the obtained values of the P-d curves according to equations (6)–(7).

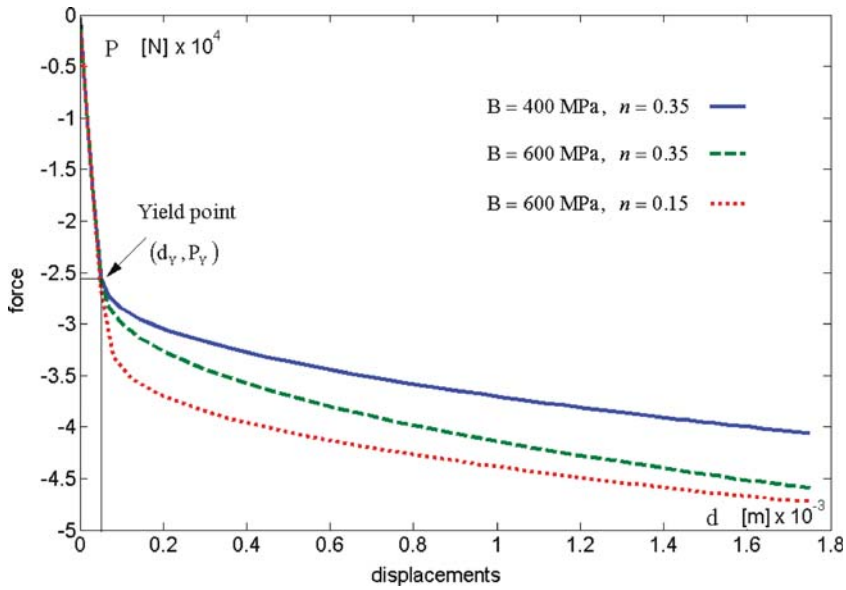

Fig. 6. The resultant load-displacement curves

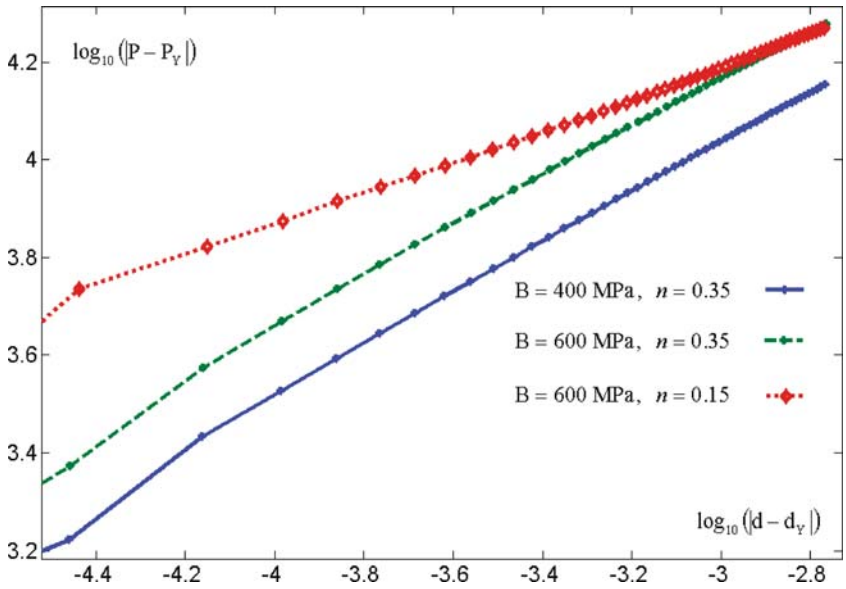

Fig. 7. The resultant load-displacement curves on a logarithmic scale

Reduction of P-d Data to $\hat{\sigma}_{eqv} - \hat{\varepsilon}_{eqv}$

In this section, we present correlations between $\hat{\sigma}_{eqv}$ and $\hat{\varepsilon}_{eqv}$ and the applied load P and displacement d respectively. The numerical analyses provide $\hat{\varepsilon}^{(i)}_{eqv}$, $\hat{\sigma}^{(i)}_{eqv}$, $P^{(i)}$ and $d^{(i)}$ where the right upper superscript (i) represent the load step number. The correlation is of the usual form $\hat{\varepsilon}_{eqv} = f\left(\frac{d}{h}\right)$ and $\hat{\sigma}_{eqv} = g\left(\frac{d}{h}, \frac{P}{Dt}\right)$. These relationships are valid for (d, P) > (d_Y, P_Y), where $h = \sqrt{2}w,t$ and D are the specimen's geometrical parameters (Fig. 1). The calculated $\hat{\varepsilon}_{eqv} = f\left(\frac{d}{h}\right)$ curves are plotted in Fig. 8 for the 3 sets of hardening parameters of Table 1. The results show a non-linear relationship between the applied displacement and the resultant strain. The numerical results of $\hat{\sigma}_{eqv} = g\left(\frac{P}{Dt}\right)$, normalized by σ_Y, are plotted in Fig. 9. It can be observed that, for $P > P_Y$, the relationship is nonlinear too.

Processing of Results

This section provides a method for the determination of B and n of the parabolic hardening equation. Firstly, it is assumed that the material properties are linearly related to the P-d characteristics by:

$$\log_{10} B = c_1 + c_2\, k + c_3(\log_{10} C) \tag{9}$$

and

$$n = d_1 + d_2\, k + d_3(\log_{10} C) \tag{10}$$

The linear assumption means that n and B are continuous functions of k and C and may be estimated using the first derivatives of a Taylor expansion. For each specimen geometry, three different P-d graphs are plotted. The three graphs correspond to three different example hardening models (Table 1). The three different P-d curves are then plotted in Fig. 7 on a log-log scale according to equation (7) The two characteristics of each straight line $\left(\log_{10} C^{(j)}, k^{(j)}, j = 1 \ldots 3\right)$ are obtained by performing a linear regression. The resulting values are listed in Table 2.

The coefficients c_i, d_i, i = 1 … 3 are then calculated by solving the following two systems of three equations

$$\begin{Bmatrix} c_1 \\ c_2 \\ c_3 \end{Bmatrix} = \mathrm{inv}\left(\begin{bmatrix} 1 & k^{(1)} & \log_{10} C^{(1)} \\ 1 & k^{(2)} & \log_{10} C^{(2)} \\ 1 & k^{(3)} & \log_{10} C^{(3)} \end{bmatrix}\right) \cdot \begin{Bmatrix} \log_{10} B^{(1)} \\ \log_{10} B^{(2)} \\ \log_{10} B^{(3)} \end{Bmatrix} \tag{11}$$

Table 2 The load-displacement coefficients $\log_{10}$ C and k in relation to the parabolic hardening l material properties $\log_{10}$ B and n

σ-ε		P-d	
$\log_{10}$ B	n	$\log_{10}$ C	k
8.6021	0.35	5.6818	0.5578
8.7782	0.35	5.7225	0.5245
8.7782	0.15	5.1542	0.3196

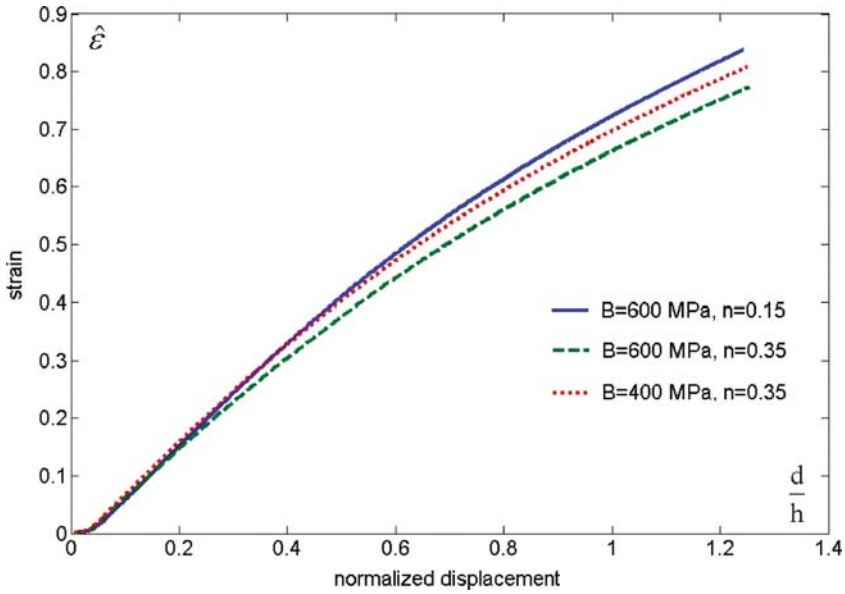

Fig. 8. The strain $\hat{\varepsilon}_{eqv}$ as a function of the applied displacement

$$\begin{Bmatrix} d_1 \\ d_2 \\ d_3 \end{Bmatrix} = \text{inv}\left(\begin{bmatrix} 1 & k^{(1)} & \log_{10} C^{(1)} \\ 1 & k^{(2)} & \log_{10} C^{(2)} \\ 1 & k^{(3)} & \log_{10} C^{(3)} \end{bmatrix} \right) \cdot \begin{Bmatrix} n^{(1)} \\ n^{(2)} \\ n^{(3)} \end{Bmatrix} \tag{12}$$

The procedure to determine the plastic parameter B and n for large strains is thus summarized as:

1. Perform an experiment with the SCS specimen and obtain the P-d data.
2. Plot the experimental P-d graph of step 1 on a log-log scale according to equation (7) and obtain its $\log_{10} C^*$ and k^* by linear regression.
3. Perform numerical analyses of the SCS specimen with three different combination of B and n of equation (1).

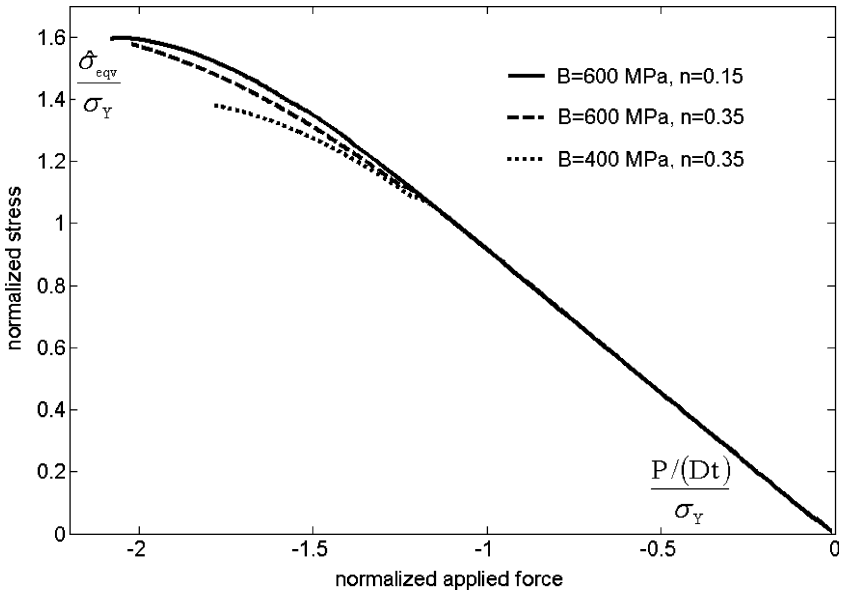

Fig. 9. The stress $\hat{\sigma}_{eqv}$ as a function of the resultant applied force

Table 3 The coefficients K_i, i = 1…3 for the 3 parabolic hardening models of Table 1 and two strain ranges

Strain range	B = 600 MPa n = 0.15	B = 600 MPa n = 0.35	B = 400 MPa n = 0.15
$\varepsilon_Y < \hat{\varepsilon} < 0.9$			
K_1	0.90	0.90	0.90
K_2	0.17	0.17	0.17
K_3	0.69	0.66	0.72
$\varepsilon_Y < \hat{\varepsilon} < 0.4$			
K_1	0.90	0.90	0.90
K_2	0.17	0.17	0.17
K_3	0.81	0.75	0.81
$\varepsilon_Y < \hat{\varepsilon} < 0.4 \quad \hat{d} = d - d_Y$			
K_1	0.92	0.92	0.92
K_2	0.17	0.17	0.17
K_3	0.90	0.84	0.90

4. Plot the three different P-d numerical graphs of step 3 on a log-log scale according to equation (7) and obtain their $\left(\log_{10} C^{(j)}, k^{(j)}, j = 1\ldots3\right)$ by a linear regression.
5. Calculate c_i, d_i, i = 1…3 using equations (11)–(12).
6. Substitute the coefficients of step 5 and $\log_{10}$ C* and k^* of step 2 into equations (9)–(10) and obtain $\log_{10}$ B* and n^*.

A proper choice of the couples (B_i, n_i, i = 1…3) of step 3 is needed. The proposed linearization will converge to the experimental parameters more rapidly when the choice of the couples (B_i, n_i, i = 1…3) is sufficiently close to the correct parameters. In order to verify the results, a fourth numerical analysis may be performed using the obtained properties. If the numerical resultant P*-d* agree with the experimental P-d data, one can conclude that a meaningful estimation of the properties has been obtained.

A Comparison with the Previous Approach Based on 3 K Coefficients

A simple stress-strain curve approximations $\hat{\varepsilon}_{eqv} = f\left(\frac{d}{h}\right)$ and $\hat{\sigma}_{eqv} = g\left(\frac{d}{h}, \frac{P}{Dt}\right)$ which uses only three coefficients K_i, i = 1…3 was originally introduced, in which [1–3]:

$$\hat{\sigma}_{eqv} = K_1\left(1 - K_2\,\hat{\varepsilon}_{eqv}\right)\frac{P}{Dt} \tag{13}$$

$$\hat{\varepsilon}_{eqv} = K_3\frac{d}{h} \tag{14}$$

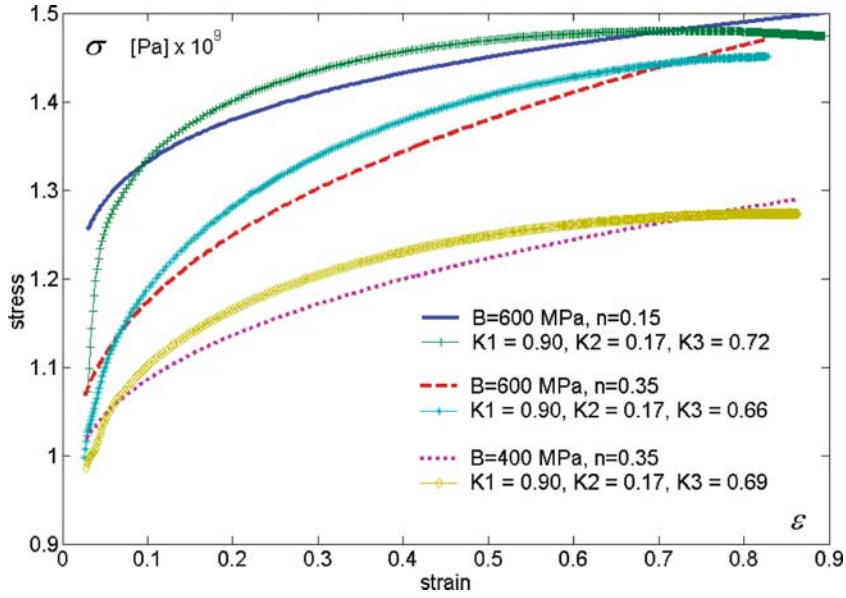

Fig. 10. A comparison of $\sigma-\varepsilon$ curves obtained by using equations (13)–(14) with the coefficient of Table 3 for $\varepsilon_Y < \varepsilon < 0.9$ and the numerical P-d curves

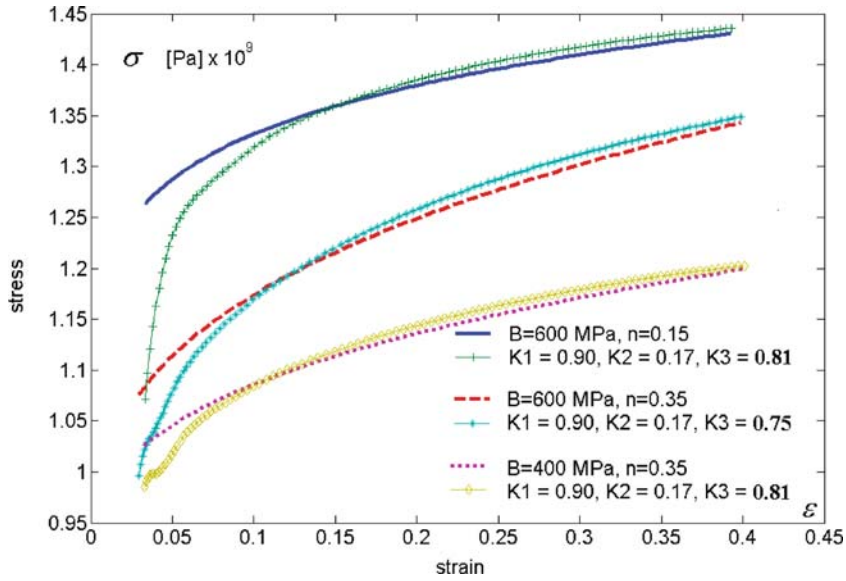

Fig. 11. A comparison of $\sigma-\varepsilon$ curves obtained by using equations (13)–(14) with the coefficient of Table 3 for $\varepsilon_Y < \varepsilon < 0.4$ and the numerical P-d curves

Since only three coefficients are involved, equations (13)–(14) are quite attractive for the experimentalist. These coefficients, once determined for a given material and gauge geometry, are used to process all the subsequent experimental data [7]. We will now examine the limits of validity of such approximations for the parabolic hardening case. Equation (14) assumes that $f\left(\frac{d}{h}\right)$ is linear with interception at $\hat{\varepsilon}_{eqv} = 0$. From Fig. 8, it is clear that for $\hat{\varepsilon}_{eqv} > \varepsilon_Y$ the interception is not at $\hat{\varepsilon}_{eqv} = 0$ and the curve is only linear for strains up to $\hat{\varepsilon}_{eqv} \approx 0.4$

The numerical stress-strain curves of Fig. 5, the load-displacements curves of Fig. 6 and equations (13)–(14) are used to determine the three coefficients K_1, K_2 and K_3 using least squares. These coefficients are calculated twice, for a strain range $\varepsilon_Y < \hat{\varepsilon}_{eqv} < 0.9$, and for a strain range $\hat{\varepsilon}_{eqv} < 0.4$. The results are summarized in Table 3.

It has been shown that the coefficients K_i, i = 1…3 depend on the geometry and the material of the SCS specimen [4]. These coefficients $K_1 = 0.90$ and $K_2 = 0.17$ were determined to be the same for all three material models. The only difference is for K_3 which varies in the range $0.66 \le K_3 \le 0.72$ for $\varepsilon_Y < \varepsilon < 0.9$, and $0.75 \le K_3 \le 0.81$ for $\varepsilon_Y < \varepsilon < 0.4$.

The $\hat{\sigma}_{eqv} - \hat{\varepsilon}_{eqv}$ curves obtained using equations (13)–(14) with the coefficient of Table 3 for $\varepsilon_Y < \varepsilon$

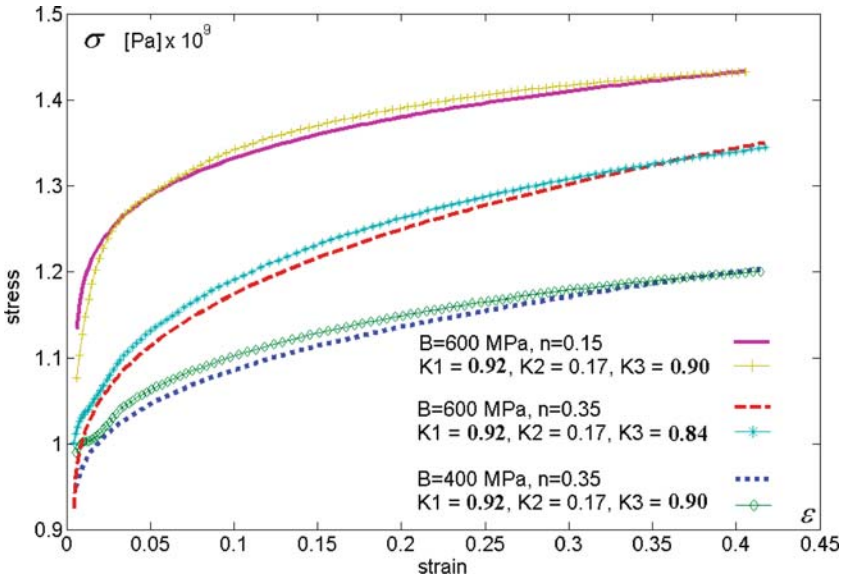

Fig. 12. A comparison of $\sigma-\varepsilon$ curves obtained by using equations (13)–(14) with the coefficient of Table 3 for $\varepsilon_Y < \varepsilon < 0.4$ and the numerical P-d curves

Table 4 Hardening moduli of the verification problems

B [MPa]	B* [MPa]	Error [%]	n	n^*	Error [%]	$\log_{10}$ C	k
500	490	−2.0	0.15	0.1564	4.2	5.1521	0.3427
500	509	1.8	0.25	0.2443	−2.3	5.4056	0.4297
500	507	1.4	0.35	0.3344	−4.5	5.6613	0.5223

o < 0.9 and the numerical P-d curves are plotted in Fig. 10. Note that the coordinates of Figs. 10–12 represent ε and $\hat{\varepsilon}_{eqv}$ and σ and $\hat{\sigma}_{eqv}$. The prescribed $\sigma-\varepsilon$ curves are also plotted for comparison. The difference in stress values $(|(\sigma - \hat{\sigma}_{eqv})/\sigma|)$ for strains $\varepsilon > 0.1$ is less than 3%. The difference in strain values at a specified stress level is greater.

Figure 11 is analogous to Fig. 10 for the range of strains of $\varepsilon_Y < \varepsilon < 0.4$. A very good agreement is observed for $0.1 < \varepsilon < 0.4$. Using equations (13)–(14) for small strains in the range $\varepsilon_Y < \varepsilon < 0.1$ is less accurate. The reason for it can be observed on Fig. 8. The linear line which can be used to correlate $\hat{\varepsilon}$ and d/h in strain range of $\varepsilon_Y < \varepsilon < 0.4$ does not intercept at $\hat{\varepsilon} = 0$. Hence a small modification is applied to equation (14)

$$\hat{\varepsilon}_{eqv} = K_3 \frac{\overline{d}}{h} \tag{15}$$

Where

$$\overline{d} = d - d_Y \tag{16}$$

And d_Y is the applied displacement at the beginning of the gage yield shown on Fig. 6.

The translation (16) influences only K_3 which lie in the range $0.84 \le K_3 \le 0.90$ and detailed in Table 3. A marked improvement of the accuracy of the simple approximation (15) and (16) can be observed in Fig. 12 for the range $\varepsilon < 0.1$ in comparison to Fig. 11. If higher accuracy is still required, a higher polynomial fit can be used such as: $\hat{\varepsilon}_{eqv} = K_4\left(\frac{\overline{d}}{h}\right)^2 + K_3\frac{\overline{d}}{h} + \varepsilon_Y$. With such a polynomial when $\overline{d} = d - d_Y = 0$, $\hat{\varepsilon}_{eqv} = \varepsilon_Y$ and the nonlinear behavior visible in Fig. 8 is fully modeled. The minor disadvantage is the need for one additional coefficient K_4.

Verification Problems

To validate the accuracy of the proposed data processing method, three additional cases were solved numerically. The cases differ in their material properties from the cases used to calculate the coefficients c_i, d_i $i = 1 \ldots 3$ of equations (9)–(10). The obtained numerical P-d data served as the "experimental measured results" input for the processing method.

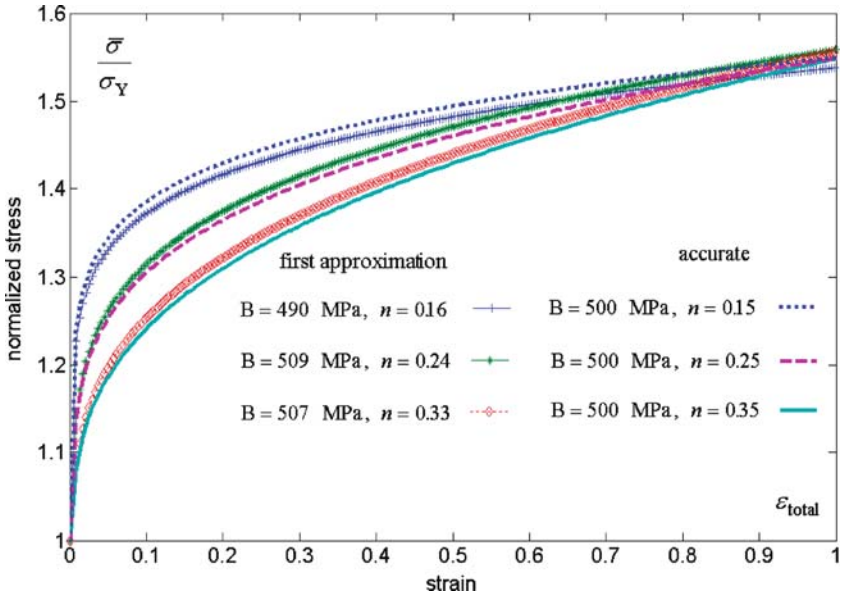

Fig. 13. A comparison between prescribed $\sigma-\varepsilon$ curves and calculated ones

First the coefficients c_i, d_i i = 1…3 are calculated using the data of Table 2 and equations (11)–(12):

$$c_i = [3.1299 \quad -3.6707 \quad 1.3235]^T \tag{17}$$

$$d_i = [-1.2045 \quad 0.2986 \quad 0.2443]^T \tag{18}$$

The "experimental" P-d curves which correspond to the properties in columns 1 and 4 of Table 4 (from left) were plotted on a log-log scale according to equation (7), with their slope and intercept determined by a linear regression. The resulting values are summarized in the last two columns of Table 4. These values together with the coefficients of equations (17)–(18) were substituted into equations (9)–(10) to obtain B* and n^*. The values are summarized in columns 2 and 5 of Table 4. The relative error [%] of this method which is calculated by (B*−B)/B and $(n^*-n)/n$ is detailed in columns 3 and 6 of Table 4.

A very good agreement between the prescribed properties and the calculated ones is obtained. The relative error is less than 4.5% for B and less than 2% for n. With the aid of equations (1)–(3) the prescribed and the calculated constitutive $\sigma-\varepsilon$ curves are plotted in Fig. 13 for stress exceeding σ_Y. The excellent agreement can again be observed in this figure.

Discussion

This paper is the continuation of previous work that dealt with the quasi-static analysis of the SCS assuming a bilinear material model. The bilinear model may be written as

$$\sigma^0 = \sigma_Y + E_p(\varepsilon_{total} - \varepsilon_Y)$$

Where E_p is the plastic modulus and

$$\varepsilon_{total} - \varepsilon_Y = \varepsilon^e + \varepsilon^p - \varepsilon_Y = \varepsilon^P + \frac{\sigma^0 - \sigma_Y}{E} \tag{20}$$

Since for large strains $\varepsilon^p >> \frac{\sigma^0-\sigma_Y}{E}$ the bilinear model may be considered as a special case of the parabolic hardening material model [equation (1)] where B = E_p and n = 1. Hence the behavior of the stress $\hat{\sigma}_{eq}$ and strain $\hat{\varepsilon}_{eqv}$ on the mid-section of the gauge is found to be similar in both investigations - they reflect the constitutive behavior of the material. Therefore, all the results pertaining to stress/strain homogeneity in bilinear case can be extended to the present parabolic case. In both cases, it was found that $\hat{\varepsilon}_{eqv} = f\left(\frac{d}{h}\right)$ is indeed non-linear but our results show that it can be linearly approximated for moderately large strains. Whereas $\hat{\sigma}_{eqv} = g\left(\frac{P}{Dt}\right)$ could be linearized for the bilinear material, the present results show a nonlinear relationship for the parabolic hardening case, as shown in Fig. 9 for $\hat{\sigma}_{eq} > \sigma_Y$.

The method for obtaining B and n can be considered as an extension of the second method described in previous investigation [4]. For the bilinear model the plastic modulus was correlated to a characteristic of the P-d curve(slope) using a second order polynomial. Here the B and n of equation (1) are correlated to the slope and intercept of the log-log P-d curve using a first order polynomial. The proposed method was shown to yield reliable estimates of B and n. An overall verification of the proposed method was brought in the form of numerical verification problems. The present work has shown that the SCS can reliably be used to investigate the mechanical behavior of parabolic hardening materials, as a generalization of the previously investigated bilinear case. While the previous approach based on three K coefficients yields valid results for moderate strain levels, additional accuracy is gained by applying the alternative method proposed here by which B and n are directly determined from the experimental load-displacement curves.

Conclusions

The applicability of the SCS to parabolic hardening materials has been investigated using numerical simulations. The influence of material parameters on the resulting stress $\hat{\sigma}_{eq}$ and strain $\hat{\varepsilon}_{eqv}$ on the mid-section of the gage has been characterized. A new method for obtaining the parabolic hardening parameters was derived and verified. The main conclusions from this work are summarized below:

- Numerical analyses show that for an SCS specimen subjected to quasi-static large deformations, the averaged $\hat{\varepsilon}_{eqv} - \hat{\sigma}_{eqv}$ on the mid-section describe the constitutive parabolic hardening of the material.
- Numerical analyses reveal that the simple approximations (13)–(15) are also valid for parabolic hardening materials.

The SCS specimen can reliably be used to determine the large strain constitutive behavior of parabolic hardening materials.

References

1. Rittel D, Ravichandran G, Lee S (2002) A shear compression specimen for large strain testing. Exp Mech 42(1):58–64.
2. Rittel D, Ravichandran G, Lee S (2002) Large strain constitutive behavior of OFHC copper over a wide range of

strain rates using the shear compression specimen. Mech Mater 34(10):627–642.
3. Vural M, Rittel D, Ravichandran G (2003) Large strain mech anical behavior of 1018 cold rolled steel over a wide range of strain rates. Metall Mater Trans A 34A(12):2873–2885.
4. Dorogoy A, Rittel D (2005) Numerical validation of the shear compression specimen. Part I: Quasi-static large strain testing. Exp Mech 45(2):167–177.
5. Dorogoy A, Rittel D (2005) Numerical validation of the shear compression specimen. Part I: Dynamic large strain testing. Exp Mech 45(2):178–185.
6. ANSYS, Release 8.0, 2005, Ansys Inc.
7. Rittel D, Levin R, Dorogoy A (2004) On the isotropy of the dynamic mechanical and failure properties of swaged tungsten heavy alloys. Metall Mater Trans A 35A:3787–3795.